

Nonlinear dynamics of Bose-condensed gases by means of a low- to high-density variational approach

Alexandru I. Nicolin*

Niels Bohr Institute, Blegdamsvej 17, Copenhagen, 2100-DK

R. Carretero-González†

Nonlinear Dynamical Systems Group‡, Department of Mathematics and Statistics,
and Computational Science Research Center, San Diego State University, San Diego CA, 92182-7720, USA

We propose a versatile variational method to investigate the spatio-temporal dynamics of one-dimensional magnetically-trapped Bose-condensed gases. To this end we employ a q -Gaussian trial wave-function that interpolates between the low- and the high-density limit of the ground state of a Bose-condensed gas. Our main result consists of reducing the Gross-Pitaevskii equation, a nonlinear partial differential equation describing the $T = 0$ dynamics of the condensate, to a set of only three equations: *two coupled nonlinear ordinary differential equations* describing the phase and the curvature of the wave-function and *a separate algebraic equation* yielding the generalized width. Our equations recover those of the usual Gaussian variational approach (in the low-density regime), and the hydrodynamic equations that describe the high-density regime. Finally, we show a detailed comparison between the numerical results of our equations and those of the original Gross-Pitaevskii equation.

I. INTRODUCTION

Due to the unprecedented experimental maneuverability of Bose-condensed gases, their intrinsically nonlinear dynamics became an appealing research topic engrossing scientists from fields as diverse as numerical analysis and condensed matter physics [1, 2, 3]. The $T = 0$ dynamics of these gases is accurately described by the so-called Gross-Pitaevskii equation (GPE), a cubic Schrödinger equation brought forward in the early sixties by two seminal papers of Gross and Pitaevskii [4, 5].

While there is good quantitative agreement between the full GPE and current experimental results on a wide range of topics, including: dark soliton dynamics inside magnetic traps [6, 7], bright soliton interactions [8], non-equilibrium oscillations in binary BECs [9], and Faraday waves in periodically driven BECs [10], there are, however, rather few models giving analytical insight. Naturally, reducing the partial-differential, therefore *infinitely-dimensional*, GPE to the level of a few ordinary differential equations (ODEs) is a nontrivial task. Previous works include the so-called Gaussian variational model (which describes the low-density regime) [11, 12, 13, 14] and the hydrodynamic analysis of high-density condensates [15, 16]. All these works addressed the dynamics of a Bose-condensed gas close to its ground state. For a comprehensive account, from both an experimental and theoretical viewpoint, of excited states such as solitons, vortices and alike we refer to the recent review [17] and references therein. In this paper we present an efficient universal variational model able

to describe both the high- and the low-density dynamics close to the ground state (*i.e.*, without entering the realm of soliton-like solutions). Our model stems from the q -Gaussian trial wave-functions that were used to describe the ground-state properties of a trapped Bose-condensed gases [18, 19, 20]. Though restricted to ground-state properties, the work of Fetter [18] is particularly relevant since he is the first one to point out the universality of this ansatz.

The rest of the paper is structured as follows: In Sec. II we present the variational method using the q -Gaussian trial wave-function. In Sec. II A we reduce the variational equations to the level of three coupled ODEs and in Sec. II B we simplify these equations to the level of two coupled nonlinear ordinary differential equations describing the phase and the curvature of the wave-function, and a separate algebraic equation yielding the generalized width. In Secs. III and IV we show that our equations recover those of the variational Gaussian model and the standard hydrodynamic formulation of the GPE. Section V presents our numerical results for a particular case of a GPE with a periodically forced nonlinearity. Finally, Sec. VI is allotted to our concluding remarks.

II. VARIATIONAL MODEL

A. Coupled equations

The equation describing the $T = 0$ dynamics of a trapped three-dimensional Bose-condensed gas is given, in adimensional units, by

$$i \frac{\partial \psi(\mathbf{r}, t)}{\partial t} = \left(-\frac{1}{2} \nabla^2 + V(\mathbf{r}) + U(t) |\psi(\mathbf{r}, t)|^2 \right) \psi(\mathbf{r}, t), \quad (1)$$

‡URL: <http://nlds.sdsu.edu>

*Electronic address: nicolin@nbi.dk

†URL: <http://rohan.sdsu.edu/~rcarretero/>

where the time-dependent nonlinearity is given by $U(t) = 4\pi a(t)$, $a(t)$ is the time-dependent two-body scattering length, and we have taken for simplicity $\hbar = m = 1$.

In this work we consider a quasi-one-dimensional Bose-Einstein condensate (BEC) confined in a strongly anisotropic magnetic trap. In such a setup the dynamics of the condensate is well-known to follow a one-dimensional version (with rescaled nonlinearity coefficient) of the three-dimensional GPE (1) [21]. Now that the system under scrutiny is one-dimensional in nature, we can consider the usual magnetic, parabolic, trapping potential of the form

$$V(x) = \frac{\Omega^2}{2}x^2. \quad (2)$$

Let us now use the following trial wave-function (from now on called the q -Gaussian) to describe the state of the condensate close to its ground state

$$\psi(x, t) = f[q(t)] \sqrt{N} \left(1 - \frac{(1-q(t))x^2}{2w(t)^2}\right)^{\frac{1}{1-q(t)}} e^{ix^2\beta(t)}. \quad (3)$$

The q -Gaussian ansatz (3) has three, free, time-dependent parameters $\{w, \beta, q\}$ corresponding, respectively, to the width (which is strictly positive at all times), chirp, and q parameter, where the q parameter captures the regime of the BEC cloud (see below). To determine $f[q(t)]$ one imposes the normalization condition

$$\int_D |\psi(x, t)|^2 dx = N, \quad (4)$$

where N represents the total number of atoms in the condensate and

$$D = \left[-\frac{\sqrt{2}w(t)}{\sqrt{1-q(t)}}, \frac{\sqrt{2}w(t)}{\sqrt{1-q(t)}} \right] \quad (5)$$

is the domain supporting the q -Gaussian ansatz. Computing the norm (4) one finds

$$f[q(t)] = \frac{(1-q(t))^{1/4}}{2^{1/4}w(t)^{1/2}B^{1/2}\left(\frac{1}{2}, \frac{-3+q(t)}{-1+q(t)}\right)}, \quad (6)$$

where $B(\cdot, \cdot)$ is the usual Euler beta function [22].

It is crucial to note the two important limits of the q -Gaussian ansatz: in the $q(t) \rightarrow 1$ limit our ansatz recovers the usual Gaussian ansatz (valid for low-density condensates), as

$$\lim_{q(t) \rightarrow 1} \left(1 - \frac{(1-q(t))x^2}{2w(t)^2}\right)^{\frac{1}{1-q(t)}} = \exp\left(\frac{-x^2}{2w(t)^2}\right) \quad (7)$$

and

$$D = (-\infty, \infty), \quad (8)$$

while the $q(t) \rightarrow -1$ limit recovers the usual parabolic density profile of the Thomas-Fermi region (valid for high-density condensates), as

$$\lim_{q(t) \rightarrow -1} \left(1 - \frac{(1-q(t))x^2}{2w(t)^2}\right)^{\frac{1}{1-q(t)}} = \sqrt{1 - \frac{x^2}{w(t)^2}} \quad (9)$$

and

$$D = [-w(t), w(t)]. \quad (10)$$

The novelty of this ansatz is that in addition to having the usual variational parameters $w(t)$ (width of the condensate) and $\beta(t)$ (chirp), it *also* accounts for the possible changes of curvature through the $q(t)$ variable. As the above limits clearly show $q(t)$ is the crucial ingredient for being able to recover analytically both the low- and the high-density regime of a BEC. Naturally, the q -Gaussian is not the only function that is able to interpolate between these two limits of a BEC [23]. The so-called S_n function

$$S_n(x) = \exp\left(-\sum_{k=1}^n \frac{x^{2k}}{k}\right) \quad (11)$$

becomes a Gaussian for $n = 1$ and turns into a parabolic profile for $n \rightarrow \infty$ (and $|x| < 1$), as

$$\begin{aligned} S_\infty(x) &= \exp\left(-\sum_{k=1}^{\infty} \frac{x^{2k}}{k}\right) \\ &= \exp(\ln(1-x^2)) = 1-x^2. \end{aligned}$$

The advantage of using the q -Gaussian lies however in the fact that this function is amenable to analytical computation (and gives rise to very simple equations describing the dynamics of the condensate), while other functions (like the $S_n(x)$) are not.

Our variational method follows the traditional recipe: we introduce the q -Gaussian trial wave-function in the BEC Lagrangian defined as

$$L(t) = \int_D \mathcal{L}(x, t) dx, \quad (12)$$

where D is given by (5) and the Lagrangian density is given by

$$\mathcal{L}(x, t) = \frac{i}{2}(\psi\psi_t^* - \psi^*\psi_t) + \frac{1}{2}|\psi_x|^2 + V(x)|\psi|^2 + \frac{U(t)}{2}|\psi|^4. \quad (13)$$

The dynamics of the BEC, restricted to our ansatz, is then determined through the Euler-Lagrange equations

$$\frac{d}{dt} \frac{\partial L}{\partial \dot{y}} = \frac{\partial L}{\partial y}, \quad (14)$$

where $y = \{w, \beta, q\}$. These equations will be the main result of our paper and, as we will confirm in the following sections, they are able to accurately describe the

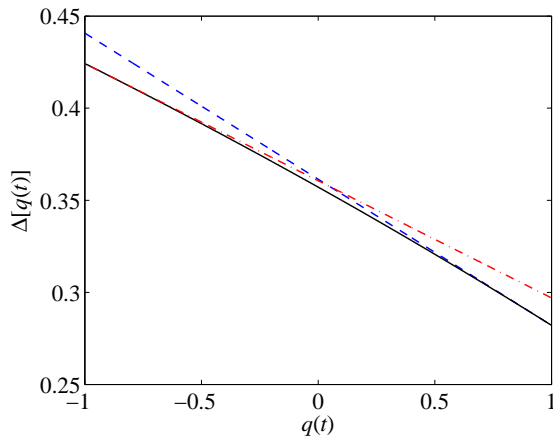


FIG. 1: (Color online) The solid black line shows $\Delta[q(t)]$ as given by Eq. (20), while the blue dashed line and the red dash-dotted line show $\Delta[q(t)]$ as given by the approximate formulas (21) and (22).

dynamics of the condensate in both the high- and the low-density limit.

A couple of straightforward (though tedious) integrations show that

$$\frac{L(t)}{N} = L_1(t) + L_2(t) + L_3(t) + L_4(t), \quad (15)$$

where

$$L_1(t) = \frac{2w(t)^2 \dot{\beta}(t)}{7 - 3q(t)}, \quad (16)$$

$$L_2(t) = \frac{NU(t)}{w(t)\sqrt{2}} \Delta[q(t)], \quad (17)$$

$$L_3(t) = \frac{w(t)^2 \Omega^2}{7 - 3q(t)}, \quad (18)$$

$$L_4(t) = \frac{5 - q(t)}{8w(t)^2(1 + q(t))} + \frac{4w(t)^2 \beta(t)^2}{7 - 3q(t)} \quad (19)$$

are the four terms of the BEC Lagrangian. The only apparently cumbersome term is L_2 which involves

$$\Delta[q(t)] = \frac{\sqrt{\pi} \Gamma\left(1 - \frac{4}{q(t)-1}\right) \sqrt{1 - q(t)}}{2B^2\left(\frac{1}{2}, \frac{q(t)-3}{q(t)-1}\right) \Gamma\left(\frac{3}{2} - \frac{4}{q(t)-1}\right)}. \quad (20)$$

A close numerical inspection of this function shows that it is, however, *almost linear*, as can be easily seen from Fig. 1.

For practical purposes one can use the two linear approximations:

$$\Delta[q(t)] = \frac{41 - 9q(t)}{64\sqrt{\pi}}, \quad (21)$$

for the low-density case and

$$\Delta[q(t)] = \frac{51 - 9q(t)}{100\sqrt{2}}, \quad (22)$$

for the high-density one. These linear approximations come from the series expansion of $\Delta[q(t)]$ around $q(t) = 1$ and -1 . It is worth mentioning that in our numerics (see Sec. V) we use the full expression (20).

Let us notice that by setting $q(t)$ to -1 the first term in L_4 diverges, a result which is perfectly consistent with the Thomas-Fermi theory, where one neglects the kinetic term, which is numerically small in the bulk of the condensate for large number of atoms, due to its divergence at the border of the cloud. As will be shown shortly, our variational method works flawlessly in the high-density limit where $q(t)$ will be close but *always larger* than -1 , therefore the divergence will never be an issue. As far as we know this is the first variational method that is able to describe dynamically the Thomas-Fermi limit.

The Euler-Lagrange equations for $\{w, \beta, q\}$ are

$$\frac{q(t) - 5}{4w(t)^3(1 + q(t))} - \frac{\Delta[q(t)] NU(t)}{\sqrt{2}w(t)^2} + 2w(t) \frac{\Omega^2 + 4\beta(t)^2 + 2\dot{\beta}(t)}{7 - 3q(t)} = 0 \quad (23)$$

$$w(t) \left(4\beta(t) - \frac{3\dot{q}(t)}{7 - 3q(t)} \right) = 2\dot{w}(t) \quad (24)$$

$$-\frac{6}{8(1 + q(t))^2 w(t)^2} + \frac{\Delta_q[q(t)] NU(t)}{\sqrt{2}w(t)} + 3w(t)^2 \frac{\Omega^2 + 4\beta(t)^2 + 2\dot{\beta}(t)}{(7 - 3q(t))^2} = 0, \quad (25)$$

where $(\cdot)_q$ stands for derivative with respect to q .

Adding an extra exponential term like $\exp(i\phi)$ in the

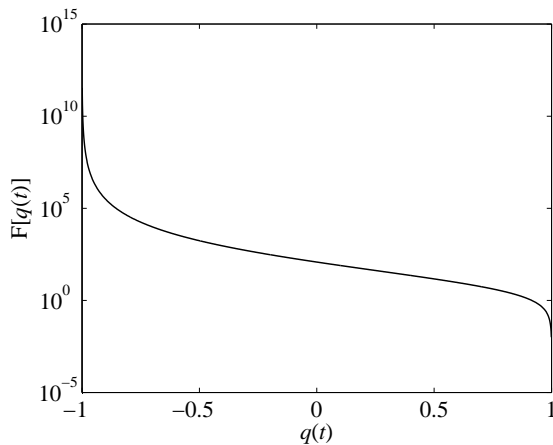


FIG. 2: The line shows $F[q(t)]$ as given by Eq. (27). To illustrate the singularity at $q(t) = -1$ we have chosen a log-plot. Please notice that outside the vicinity of $q(t) = -1$ $F[q(t)]$ is numerically well behaved. Notice as well that $F[q(t)]$ has an infinite slope at $q(t) = \pm 1$.

trial wave-function, *i.e.*, extending the set of variables to $\{N, \phi, w, \beta, q\}$, gives rise to $\dot{N} = 0$, the equation assuring the conservation of the norm, and $\dot{\phi} = 0$, but leaves the previous equations unchanged. We have dropped this term for simplicity. Naturally, one can imagine various other corrections to the present ansatz. However, even simple phase corrections such as $\exp(i\gamma_n(t)x^n)$, where n is an even integer strictly bigger than two, yield an analytically intractable Lagrange function.

While Eqs. (23)–(25) are relatively simple to write down, they are in fact *differential-algebraic equations* and (if left in their current form) require specialized numerical treatment (see, for instance, the monograph of Hairer *et al.* [24]).

To understand the nature of this dynamical system let us remember that variational methods are usually build around *pairs of canonically conjugated variables*, which give rise to coupled ODEs. Taking, for example, the simple case of $q = 1$ one easily notices that $p = w^2/2$ (the generalized momentum) and $q = \beta$ (the generalized coordinate) are the two canonically conjugate variables. Our ansatz, however, does not possess this intrinsic symmetry, as q has no canonical conjugate, which finally gives rise to the algebraic constraint. Since the Lagrange function becomes analytically intractable at the slightest change in the ansatz, it is unfruitful to try working with pairs of conjugate variables. This latter option requires the use of a direct method [25], which has the same lack of transparency as the numerical solution of the original GPE. Instead, in order to gain analytical insight, one can easily decouple the previous equations, a task which is detailed in the next subsection.

B. Decoupled equations

In order to simplify the numerical solution of equations Eq. (23)–(25) one multiplies Eq. (23) by $3w(t)/2(7-3q(t))$ and then subtracts it from Eq. (24). The ensuing equation is purely algebraic. Its solution with respect to $w(t)$ is

$$w(t) = \frac{F[q(t)]}{NU(t)}, \quad (26)$$

where

$$F[q(t)] \equiv \frac{\sqrt{2}}{(1+q(t))} \left(\frac{7-3q(t)}{2(1+q(t))} + \frac{q(t)-5}{4} \right) \frac{1}{\left\{ \frac{2}{3}\Delta_q[q(t)](7-3q(t)) + \Delta[q(t)] \right\}}. \quad (27)$$

Equation (26) can now be used in the other two equations. We have now decoupled the equation of the width, $w(t)$, from those of $q(t)$ and $\beta(t)$. A close numerical inspection of $F[q(t)]$ shows that it has a singularity at $q(t) = -1$ (which, as mentioned before, follows physically from the divergence of the kinetic energy at the border of the cloud), and is (numerically) well behaved everywhere else as one can easily infer from Fig. 2.

The original variational equations (23)–(25) can now be recast as

$$\dot{q}(t) = \frac{2\frac{\dot{U}(t)}{U(t)} + 4\beta(t)}{2\frac{F_q[q(t)]}{F[q(t)]} - \frac{3}{3q(t)-7}}, \quad (28)$$

for $q(t)$ and

$$\dot{\beta}(t) = -2\beta^2 - \frac{\Omega^2}{2} + G[q(t)]N^4U(t)^4, \quad (29)$$

for $\beta(t)$, where

$$\begin{aligned} G[q(t)] &\equiv (5-q(t) + 2\sqrt{2}\Delta[q(t)]F[q(t)](1+q(t))) \\ &\quad \times (7-3q(t))F^{-4}[q(t)](1+q(t))^{-1}/16 \\ &= \{3\Delta[q(t)] + 2\Delta_q[q(t)](7-3q(t))\}^3(7-3q)^2 \\ &\quad \times \{3\Delta[q(t)] - \Delta[q(t)](q(t)-5)(1+q(t))\} \\ &\quad \times 8(1+q(t))^6(q(t)-9)^{-4}(q(t)-1)^{-4}/81. \end{aligned}$$

Equations (28) and (29) constitute the main theoretical result of our work.

Before going into the high- and low-density limits of these two equations let us make the following comment: the dynamics of $q(t)$ depends only *indirectly* on the number of particles. It is therefore extremely instructive to analyze the denominator in Eq. (28)

$$E[q(t)] = 2\frac{F_q[q(t)]}{F[q(t)]} - \frac{3}{3q(t)-7}, \quad (30)$$

see Fig. 3, and notice that *it diverges* in the vicinities of $q(t) = \pm 1$ and is well behaved everywhere else. Let us

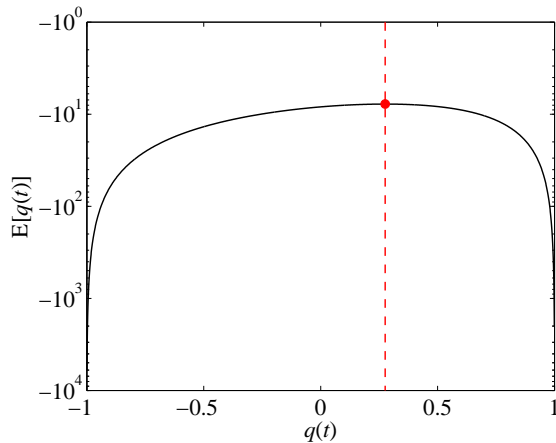


FIG. 3: (Color online) The line shows $E[q(t)]$. The divergence around $q(t) = \pm 1$ indicates that the low- and the high-density regimes have a very weak surface dynamics, *i.e.*, $\dot{q}(t) \approx 0$. The red dot (of coordinates $(q_c, E[q_c]) = (0.27605\dots, -7.76722\dots)$) and the accompanying dashed red line (of equation $q = q_c = 0.27605$) indicate the extremum value of $E[q(t)]$ at q_c .

notice that the extremum value of $E[q(t)]$ corresponds

$$\dot{q}(t) = \left(2 \frac{\dot{U}(t)}{U(t)} + 4\beta(t) \right) \left[\frac{3}{7-3q(t)} + \frac{2}{q(t)-9} + \frac{2}{q(t)-1} - \frac{6}{1+q(t)} \right]^{-1} \quad (31)$$

and

$$\dot{\beta}(t) = -\beta(t)^2 - \frac{\Omega^2}{2} + \frac{2187}{5} \frac{(q(t)-4)(q(t)-3)(1+q(t))^9(3q(t)-7)^2}{10^7(9-10q(t)+q(t)^2)^4} N^4 U(t)^4. \quad (32)$$

As $F[q(t)]$ reduces to

$$F[q(t)] = \frac{50(q(t)-9)(q(t)-1)}{9(1+q(t))^2}, \quad (33)$$

and we are investigating the dynamics of the system in a vicinity of $q(t) = -1$, Eqs. (31) and (32) take the simpler form

$$\dot{q}(t) = - \left(2 \frac{\dot{U}(t)}{U(t)} + 4\beta(t) \right) \left[\frac{9}{10} + \frac{6}{1+q(t)} \right]^{-1} \quad (34)$$

and

$$\dot{\beta}(t) = -\beta(t)^2 - \frac{\Omega^2}{2} + \frac{3NU(t)}{4w(t)^3}. \quad (35)$$

to $q_c \approx 0.27605\dots$. The divergence of $E[q(t)]$ originates from the infinite slope of $F[q(t)]$ at $q(t) = \pm 1$ and indicates that $\dot{q}(t) \approx 0$ or, in other words, that in both the low- and the high-density regime the dynamics of a BEC affects only *superficially* the curvature of the wave function. This shows in turn why the use of a Gaussian ansatz in the Thomas-Fermi regime gives rise to quantitatively good results (see, for instance, Ref. [13]). The main point we want to stress is that these two *physically different* regimes have in common a very weak surface dynamics, therefore almost any ansatz with an intrinsic breathing mode provides decent quantitative results.

Finally, let us notice that the Jacobi matrix of the dynamical system made out of Eqs. (28) and (29) (computed with the ground state values of q and β and, of course, constant U) has complex conjugate roots throughout the whole density spectrum.

III. HIGH-DENSITY CONDENSATES

To see how the previous equations recover the usual hydrodynamic formulation let us consider for $\Delta[q(t)]$ the approximation given by Eq. (22). Within this approximation we have that

Equation (35) along with the Eq. (24), where we now ignore the time derivative of $q(t)$, *i.e.*,

$$\dot{w}(t) = 2w(t)\beta(t), \quad (36)$$

are the so-called hydrodynamic equations. To see this more clearly let us work in the variables $\alpha(t)$ and $a(t)$ defined as

$$\beta(t) = \frac{\alpha(t)}{2} \quad (37)$$

and

$$a(t) = -\frac{3N}{4w(t)^3}, \quad (38)$$

so that equations (31) and (32) read

$$\begin{aligned} \dot{a}(t) + 3\alpha(t)a(t) &= 0 \\ \dot{\alpha}(t) + \alpha(t)^2 + \Omega^2 + 2U(t)a(t) &= 0. \end{aligned} \quad (39)$$

These are exactly the hydrodynamic equations put forward by Dalfovo *et al.* [16].

IV. LOW-DENSITY CONDENSATES

A. Gaussian ansatz

In the low-density limit one can set $q(t)$ to 1 and ignore its derivative with respect to time, in which case Eqs. (23)–(25) can be recast as

$$\begin{aligned} -\frac{1}{2w(t)^3} - \frac{NU(t)}{2\sqrt{2\pi}w(t)^2} + \frac{\Omega^2 w(t)}{2} \\ + 2w(t)\beta(t)^2 + w(t)\dot{\beta}(t) = 0 \\ 2w(t)\beta(t) = \dot{w}(t). \end{aligned} \quad (40)$$

From the second equation in (40) one has that

$$\ddot{w}(t) = 4w(t)\beta(t)^2 + 2w(t)\dot{\beta}(t), \quad (41)$$

therefore

$$\ddot{w}(t) - \frac{1}{w(t)^3} - \frac{NU(t)}{\sqrt{2\pi}w(t)^2} + \Omega^2 w(t) = 0. \quad (42)$$

This is the well-known equation that describe the dynamics of the width of the condensate in the low-density limit.

B. q -Gaussian ansatz

One way to refine the standard equation stemming from the Gaussian ansatz is to start from Eqs. (28) and (29) and use for $\Delta[q(t)]$ the high-density approximation provided by Eq. (21). The ensuing equations are

$$\dot{q}(t) = \left(2\frac{\dot{U}(t)}{U(t)} + 4\beta(t) \right) \left[\frac{2}{q(t)-9} + \frac{2}{q(t)-1} - \frac{4}{1+q(t)} + \frac{3}{7-3q(t)} + \frac{18}{1-9q(t)} \right]^{-1} \quad (43)$$

and

$$\dot{\beta}(t) = -\beta^2 - \frac{\Omega^2}{2} + \frac{(7-3q(t))^2(1+q(t))^6(9q(t)-1)^3(26+3(q(t)-7)q(t))}{2097152\pi^2(q(t)-9)^4(q(t)-1)^4} N^4 U(t)^4. \quad (44)$$

As $F[q(t)]$ reduces to

$$F[q(t)] = \frac{16\sqrt{2\pi}(q(t)-9)(q(t)-1)}{(1+q(t))^2(9q(t)-1)}, \quad (45)$$

and we are investigating the dynamics of the system in a vicinity of $q(t) = 1$, Eqs. (43) and (44) take the simpler form

$$\dot{q}(t) = \frac{q(t)-1}{2} \left(2\frac{\dot{U}(t)}{U(t)} + 4\beta(t) \right) \quad (46)$$

and

$$\dot{\beta}(t) = -\beta(t)^2 - \frac{\Omega^2}{2} - \frac{1}{2w(t)^4} - \frac{NU(t)}{u(q)\sqrt{2\pi}w(t)^3}, \quad (47)$$

where

$$u(q) = \frac{128}{142 - 81q(t) + 27q(t)^2}. \quad (48)$$

Replacing in Eq. (45) $q(t)$ with 1 in all factors except the one yielding a zero term, one has that

$$q(t) = 1 - \frac{NU(t)w(t)}{4\sqrt{2\pi}}. \quad (49)$$

Finally, inserting $q(t)$ in Eq. (46) one has that

$$\dot{w}(t) = 2w(t)\beta(t). \quad (50)$$

Except for the $u(q)$ factor Eqs. (47) and (50) are identical to Eqs. (40). Of course, the two sets of equations coincide in the $N = 0$ limit, but otherwise the ones stemming from the q -Gaussian ansatz have the clear advantage of accounting for the change in the curvature of the wave-function.

V. NUMERICAL RESULTS

In the previous two sections we have shown that the equations stemming from the q -Gaussian ansatz recover those of the usual Gaussian approach (in the low-density regime) and the standard high-density hydrodynamic

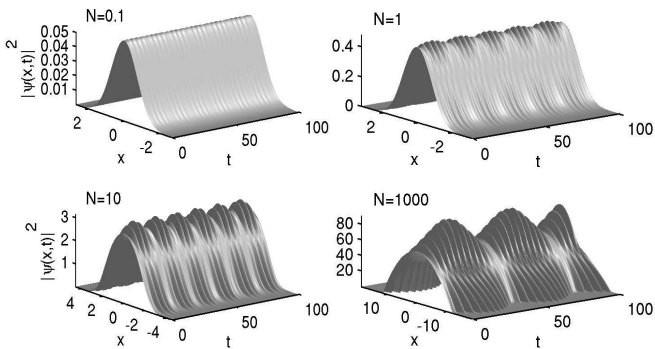


FIG. 4: Dynamics of the BEC density profile under the modulation of the nonlinearity for different atom numbers N (as indicated on each plot). Parameter values correspond to: $\Omega = 1$, $U_0 = 1$, $\epsilon = 0.1$ and $\omega = 1.6$.

equations. We now turn to a detailed numerical comparison between our variational equations and the original GPE. To this end, we consider a magnetic trap of the form (2) and a modulated nonlinear term $U(t) = U_0(1 + \epsilon \sin(\omega t))$. The modulation of the nonlinear term can be achieved by modulation of the transverse width (see Ref. [10] and references therein) or by, the so-called, Feshbach resonance technique [26, 27].

For illustration purposes we choose a magnetic trap with $\Omega = 1$ and a nonlinearity modulation with $U_0 = 1$, $\epsilon = 0.1$ and $\omega = 1.6$. Let us notice that the natural frequency of the condensate is equal to $\Omega\omega_N$, where ω_N depends weakly on N and is numerically close to 2, therefore choosing $\omega = 1.6$ assures a series of beats (or, technically, parametric resonances) between the frequency of the driving field and the natural frequency of the condensate as it can be observed in the space-time plots of the density for different values of N in Fig. 4 (for a more detailed analysis of mode-locking and energy transfer due to resonances see Refs. [28] and [29] and references therein).

The advantage of our approach is that close to resonance a system responds strongest to excitations, therefore this is the ideal setup to investigate the limits of our equations. In order to probe the different regimes of the condensate we choose five different cases corresponding to $N = 0.1, 1, 10, 10^2, 10^3$. These cases encompass the bulk part of the density spectrum, the corresponding values of q (restricted to only three significant digits) being equal to 0.990, 0.906, 0.431, -0.236 , and -0.710 , respectively. In Figs. 5 and 6 we depict, for various values of N , the steady state solution $u(x)$ to the GPE alongside the best linear square fits using the q -Gaussian, the traditional Gaussian (see Fig. 5) and the parabolic Thomas-Fermi approximation (see Fig. 6). The steady state $u(x)$ of Eq. (1) is obtained by taking

$$\psi(x, t) = u(x)e^{-i\mu t}$$

where μ is the so-called chemical potential. The ensuing steady state equation is then solved using a fixed point

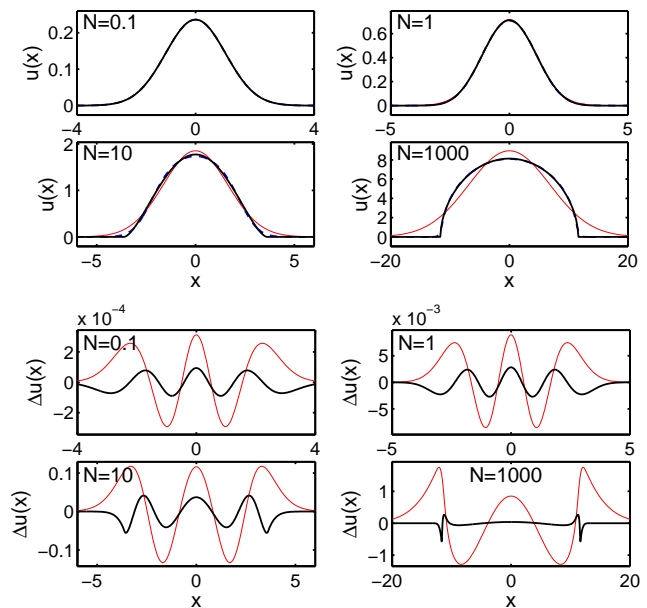


FIG. 5: (Color online) Comparison between the GPE steady state solution, the q -Gaussian fit and the Gaussian fit. The top four panels show the steady state solution to the GPE (thick black dashed line), its fit using the q -Gaussian (thick black solid line, almost indistinguishable from the dashed line due to the very good approximation) and the traditional Gaussian (thin red solid line) for different atom numbers N . The bottom four panels show the respective differences between the steady state and the q -Gaussian (thick black line) and the steady state and the traditional Gaussian (thin red line).

iteration algorithm (Newton method) by optimizing μ to give the desired total mass. In Figs. 5 and 6 we also depict (see lower set of panels) $\Delta u(x) = u_{\text{GPE}}(x) - u_{\text{fit}}(x)$, *i.e.*, the difference between the actual steady state of the GPE and the corresponding fits. As it can be clearly seen from both figures, the q -Gaussian provides an extremely good approximation of the wave-function in *both* the low- and the high-density regimes. In fact, as it can be evidence from Fig. 5, even in the low-energy regime, where it is well known that the traditional Gaussian ansatz is a good approximation, the q -Gaussian is superior. Incidentally the same is true when analyzing the high-density regime where, as it can be evidence from Fig. 6, the q -Gaussian provides a better approximation than the Thomas-Fermi profile.

To quantify the accuracy of our variational treatment of the GPE we will follow two distinct veins: *i.*) we fit the spatial component of the time-dependent density profile provided by a GPE solver with a q -Gaussian profile and compare the ensuing time-series for $f^2[q(t)]$, $w(t)$, and $q(t)$ with the corresponding ones obtained from Eqs. (23)–(25); also, we compute the full width at half maximum (FWHM), $w_{\text{FWHM}}(t)$, as a function of time both for the density profile provided by the GPE solver and that obtained from Eqs. (23)–(25); *ii.*) using two dif-

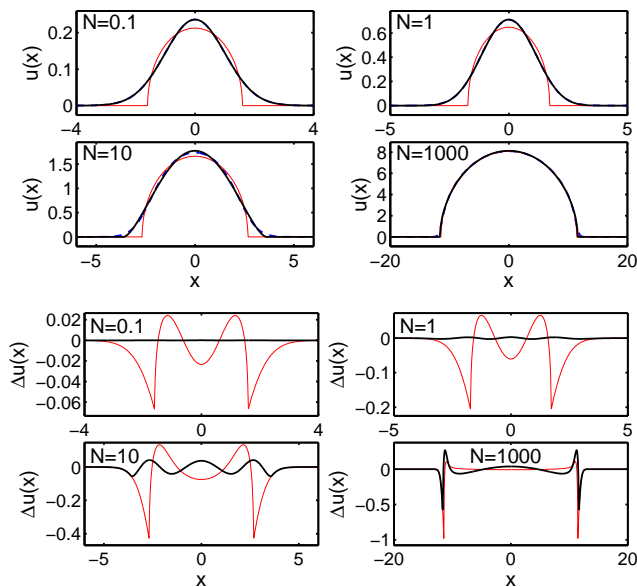


FIG. 6: (Color online) Comparison between the GPE steady state solution, the q -Gaussian fit and the parabolic Thomas-Fermi profile fit. The panels show the same information as in Fig. 5. by replacing the traditional Gaussian by the parabolic Thomas-Fermi profile.

ferent fits based on a Gaussian and a Thomas-Fermi density profile, and the q -Gaussian profile that yields from Eqs. (23)–(25), we calculate the time-dependent mean square deviation (MSD) of these profiles from that obtained from the original GPE.

Figs. 7, 8, and 9 depict the $f^2[q(t)]$, $w(t)$, and $q(t)$ time-series for, respectively, the low-density regime ($N = 0.1, 1$), the high-density regime ($N = 10^2, 10^3$), and the intermediate density regime ($N = 10$). Notice the very good agreement for $f^2[q(t)]$ and $w(t)$ for all the cases under consideration.

In the low density limit, when the condensate cloud is close to a Gaussian profile, one can observe from Fig. 7 that the dynamics of the parameter q for the full GPE numerics and the reduced ODE system are in good agreement. However, in the high- and intermediate density limits, as it can be evidenced from Figs. 8 and 9, there seems to be a (somewhat counterintuitive) poor agreement in the q time-series despite the fact that $f^2[q(t)]$ and $w(t)$ are still in very good agreement. This apparent shortcoming should not be seen as a fault of our variational treatment, but rather as an indication of the fitting sensitivity of the q -component of our density profile. In fact, we have observed that even the addition of small quantities of noise ($< 5\%$) to the profile to be fitted induce sizeable changes in the resulting q value (results not shown here). To understand this more clearly one should look into how the fitting procedure works: when minimizing the mean-square deviation between the GPE profile and the q -Gaussian one encounters the derivative of the q -Gaussian with respect to q which has a log-type of singularity at the border of the cloud. This singularity

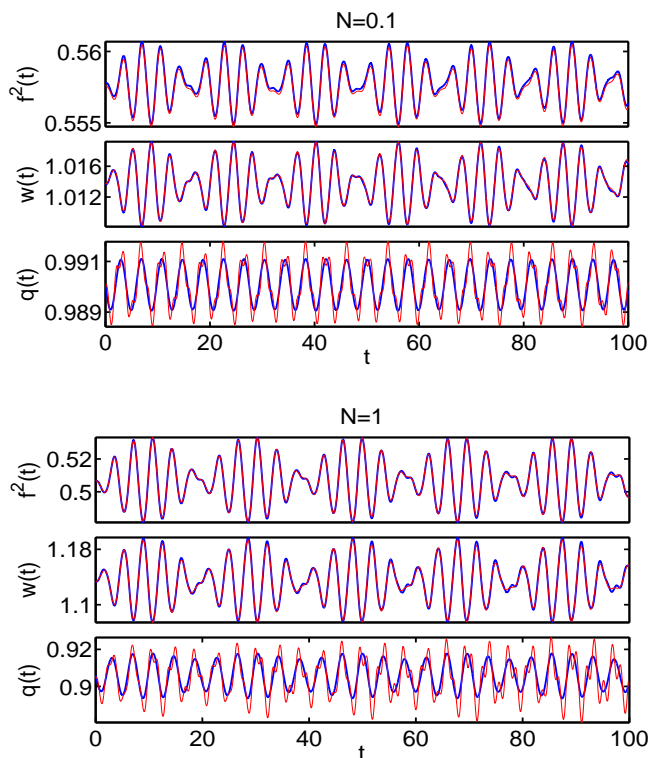


FIG. 7: (Color online) Low-density regime. Comparison between the full GPE dynamics and the reduced ODE dynamics using the q -Gaussian approach. The top (bottom) series of panels corresponds to atom numbers $N = 0.1$ ($N = 1$). For each atom number, the three panels corresponds to, from top to bottom, the time-series of a) the peak density $f^2[q(t)]$, b) width $w(t)$, and c) the q -Gaussian parameter $q(t)$. Thick blue lines corresponds to the full GPE dynamics while thin red lines to the reduced ODE dynamics using the q -Gaussian variational approach. Note that for $f^2[q(t)]$ and $w(t)$ the time-series obtained from the full GPE dynamics and our ODE reduction are practically indistinguishable.

makes it very hard to make a one-to-one comparison of $q(t)$. One way to avoid this problem is to compute $q(t)$ (via Eq. (26)) from the $w(t)$. This latter approach (see Fig. 10) shows good agreement between the two time-series.

Another way to test the quality of the q -Gaussian ansatz is to make a direct comparison between the $w_{\text{FWHM}}(t)$ time-series (see Fig. 11). The $w_{\text{FWHM}}(t)$ of the GPE density profile is computed numerically, while that of the q -Gaussian is given by

$$w_{\text{FWHM}}(t) = \frac{2\sqrt{-2 + 2^{1/2(1+q(t))}}}{\sqrt{-1 + q(t)}} w(t). \quad (51)$$

Please notice the trivial limits $q(t) \rightarrow 1$ and $q(t) \rightarrow -1$, in which cases we get the well-known results $w_{\text{FWHM}}(t) = 2\sqrt{\log 2} w(t)$ and $w_{\text{FWHM}}(t) = \sqrt{2} w(t)$.

In order to further substantiate the quality of the q -Gaussian approach we depict in Fig. 12 the mean square

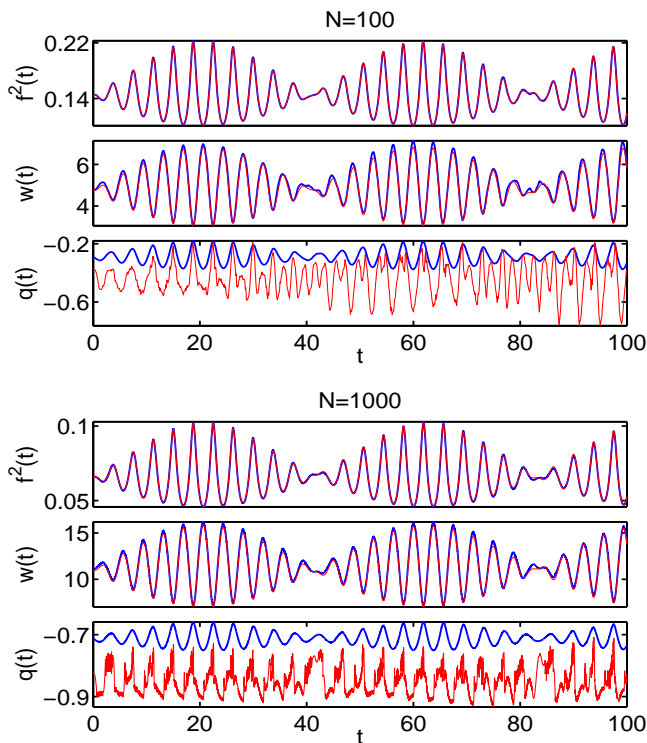


FIG. 8: (Color online) High-density regime. All panels depict same information as in Fig. 7 but in this case for $N = 10^2$ and $N = 10^3$.

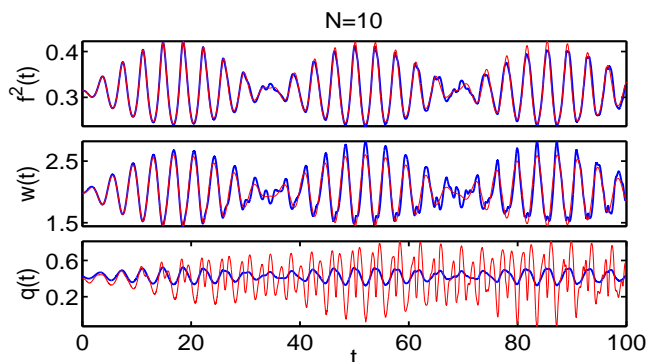


FIG. 9: (Color online) Intermediate density regime. All panels depict same information as in Fig. 7 but in this case for $N = 10$.

deviation between the different fits (note the logarithmic scale in the vertical axis). In the low-density regime the q -Gaussian function performs some four orders of magnitude better than the Thomas-Fermi fit. This result is rather obvious since the Thomas-Fermi limit is not the correct limit to use in this case. However, when comparing the q -Gaussian (blue solid line) with the traditional Gaussian (red dashed line) one can still notice more than one order of magnitude better agreement for the q -Gaussian trial function. On the other extreme of the regime (*i.e.*, the high-density regime), the q -Gaussian

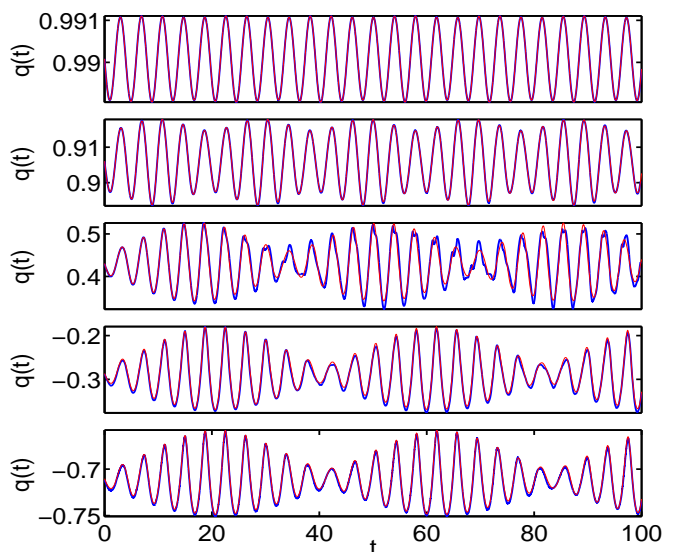


FIG. 10: (Color online) Comparison of the q -Gaussian parameter $q(t)$ between full GPE dynamics (thick blue line) and the reduced ODE dynamics by fitting $q(t)$ from $w(t)$ (thin red line). Each panel, from top to bottom, corresponds to: a) $N = 10^{-1}$, b) $N = 10^0$, c) $N = 10^2$, d) $N = 10^3$, and e) $N = 10^4$.

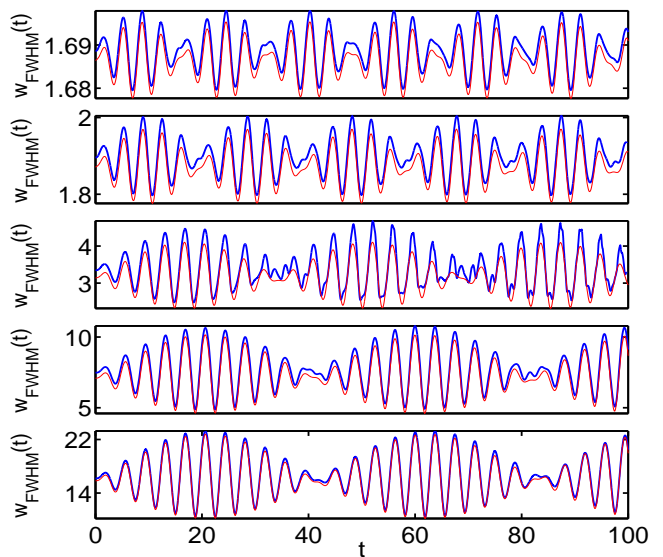


FIG. 11: (Color online) Full width at half maximum $w_{\text{FWHM}}(t)$. Each panel, from top to bottom, corresponds to: a) $N = 10^{-1}$, b) $N = 10^0$, c) $N = 10^2$, d) $N = 10^3$, and e) $N = 10^4$. Thick blue lines corresponds to the full GPE dynamics while thin red lines to the reduced ODE dynamics using the q -Gaussian variational approach.

performs about two orders of magnitude better than the traditional Gaussian. This is again obvious since the traditional Gaussian is not the right limit to use in this regime. On the other hand, it is interesting to note that the q -Gaussian has a similar performance to the Thomas-Fermi approximation in this high-density regime. Finally,

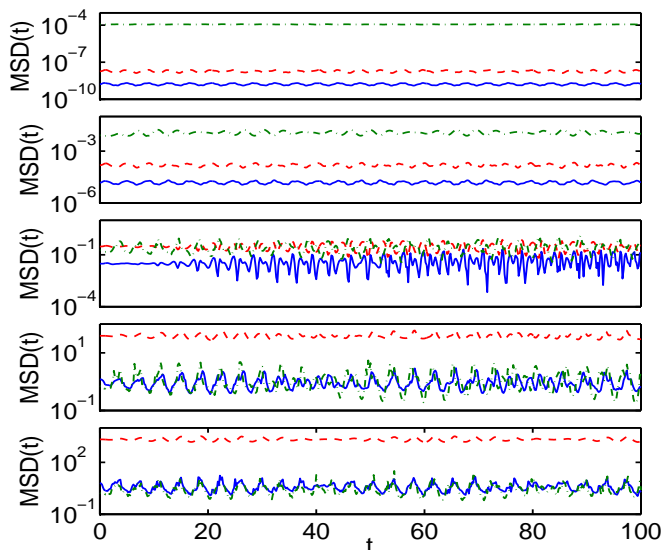


FIG. 12: (Color online) Mean square deviation (MSD) between the densities profiles obtained from the different fits and the density obtained from the original GPE. The blue solid line corresponds to the q -Gaussian approach, while the red dashed line corresponds to the traditional Gaussian and the green dash-dotted corresponds to the TF approximation. As in Fig. 10, each panel, from top to bottom, corresponds to: a) $N = 10^{-1}$, b) $N = 10^0$, c) $N = 10^2$, d) $N = 10^3$, and e) $N = 10^4$.

in the interesting, and more challenging, case of intermediate density $N = 10$, where the condensed cloud profile is neither close to Gaussian nor parabolic, the q -Gaussian clearly outperforms *both* the traditional Gaussian and the parabolic Thomas-Fermi approximation by about one order of magnitude.

Therefore, the results presented above, are clear evidence that not only the q -Gaussian is able to provide a good variational ODE reduction of the full GPE across *all* the different density regimes, but it is also has a better (or equal) performance than the separate, traditional, approximations at either extreme of the density regime.

VI. CONCLUSIONS

In this paper we have proposed an efficient variational method to investigate the spatio-temporal dynamics of

magnetically-trapped Bose-condensed gases. To this end we have employed a q -Gaussian trial wave-function that interpolates between the low- and the high-density limit of the ground state of a Bose-condensed gas. Our main result consists of reducing the Gross-Pitaevskii equation to a set of only three equations: *two coupled nonlinear ordinary differential equations* describing the phase and the curvature of the wave-function and *a separate algebraic equation* yielding the generalized width. On the analytical side our equations recover those of the usual Gaussian variational approach (in the low-density limit), and the hydrodynamic equations that describe the high-density case. On the numerical side, we have presented a detailed comparison between the numerical results of our reduced equations and those of the original GPE for the case of periodically driven BEC. We used as indicators of the q -Gaussian performance the fitting of the peak density, the condensate width, and $q(t)$, a direct comparison between the full width at half maximum obtained from our variational treatment and that of the original equation, and the mean square deviation calculations. All these indicators demonstrate that the q -Gaussian variational reduction performs very well over all the density regimes. Furthermore, we found that a) in the low-density regime, the q -Gaussian clearly outperforms the traditional Gaussian; b) in the high-density limit the q -Gaussian has a similar performance to the Thomas-Fermi approximation; c) and that in the intermediate density regime the q -Gaussian clearly outperforms *both* the traditional Gaussian and the Thomas-Fermi approximation.

Finally, let us mention that while our equations are one-dimensional they can be easily extended to two- and three-dimensional clouds. This avenue is currently under investigation and will be reported elsewhere.

Acknowledgments

The authors thank Mogens H. Jensen, Henrik Smith, Christopher Pethick and Poul Olesen for fruitful discussions on the subject. A.I.N. acknowledges the hospitality of San Diego State University where part of this work was carried out. R.C.G. acknowledges support from NSF-DMS-0505663.

[1] C. J. Pethick and H. S. Smith, *Bose-Einstein Condensation in Dilute Gases*, Cambridge University Press, Cambridge, 2002.
 [2] B. A. Malomed, *Soliton Management in Periodic Systems*, Springer-Verlag, Berlin, 2006.
 [3] P.G. Kevrekidis, D.J. Frantzeskakis, and R. Carretero-González (eds). *Emergent Nonlinear Phenomena in*

Bose-Einstein Condensates: Theory and Experiment. Springer Series on Atomic, Optical, and Plasma Physics, Vol. **45**, 2008.
 [4] L. P. Pitaevskii, *Zh. Eksp. Teor. Fiz.* **40**, 646 (1961).
 [5] E. P. Gross, *Nuovo Cimento* **20**, 454 (1961).
 [6] S. Burger, K. Bongs, S. Dettmer, W. Ertmer, K. Sengstock, A. Sanpera, G.V. Shlyapnikov, and M. Lewenstein,

- Phys. Rev. Lett. **83**, 5198 (1999).
- [7] J. Denschlag, J. E. Simsarian, D. L. Feder, Charles W. Clark, L. A. Collins, J. Cubizolles, L. Deng, E. W. Hagley, K. Helmerson, W. P. Reinhardt, S. L. Rolston, B. I. Schneider, and W. D. Phillips. *Science* **287**, 97 (2000).
- [8] U. Al Khawaja, H. T. C. Stoof, R. G. Hulet, K. E. Strecker, and G. B. Partridge, *Phys. Rev. Lett.* **89**, 200404 (2002).
- [9] K.M. Mertes, J. Merrill, R. Carretero-González, D.J. Frantzeskakis, P.G. Kevrekidis and D.S. Hall, *Phys. Rev. Lett.* **99**, 190402 (2007).
- [10] A. I. Nicolin, R. Carretero-González, and P.G. Kevrekidis, *Phys. Rev. A* **76**, 063609 (2007).
- [11] The Gaussian variational model stems from nonlinear optics, where an equation that is mathematically identical to the GPE was used to describe the propagation of light pulses. To fathom the original calculations one can look into: E. Caglioti, S. Trillo, S. Wabnitz, B. Crosignani, and P. Di Porto, *J. Opt. Soc. Am. B* **7**, 374 (1990); M. Desaix, D. Anderson, and M. Lisak, *J. Opt. Soc. Am. B* **8**, 2082 (1991); B. Crosignani, P. Di Porto, and S. Piazzolla, *Pure Appl. Opt.* **1**, 7 (1992).
- [12] B. A. Malomed, *Prog. Opt.* **43**, 71 (2002).
- [13] V. M. Pérez-García, H. Michinel, J. I. Cirac, M. Lewenstein, and P. Zoller, *Phys. Rev. Lett.* **77**, 5320 (1996).
- [14] J. J. García-Ripoll and V. M. Pérez-García *Phys. Rev. A* **59**, 2220 (1999).
- [15] S. Stringari, *Phys. Rev. Lett.* **77**, 2360 (1996).
- [16] F. Dalfovo, C. Minniti, S. Stringari, L. Pitaevskii, *Phys. Lett. A* **227**, 259 (1997).
- [17] P.G. Kevrekidis, D.J. Frantzeskakis, and R. Carretero-González (eds). *Emergent Nonlinear Phenomena in Bose-Einstein Condensates: Theory and Experiment*. Springer Series on Atomic, Optical, and Plasma Physics, Vol. **45**, 2008.
- [18] A. L. Fetter, *J. Low. Temp. Phys.* **106**, 643 (1997).
- [19] K. S. Fa, R. S. Mendes, P. R. B. Pedreira, and E. K. Lenzi, *Physica A* **295**, 242 (2001).
- [20] E. Erdemir and B. Tanatar, *Physica A* **322**, 449 (2003).
- [21] P. G. Kevrekidis and D. J. Frantzeskakis, *Mod. Phys. Lett. B* **18**, 173 (2004); V. M. Pérez-García, H. Michinel and H. Herrero, *Phys. Rev. A* **57**, 3837 (1998); L. Salasnich, A. Parola and L. Reatto, *Phys. Rev. A* **65**, 043614 (2002); Y. B. Band, I. Towers, and B. A. Malomed, *Phys. Rev. A* **67**, 023602 (2003); for a rigorous derivation of the one-dimensional model see E. H. Lieb, R. Seiringer, and J. Yngvason *Phys. Rev. Lett.* **91**, 150401 (2003).
- [22] I. S. Gradshteyn and I. M. Ryzhik, *Table of Integrals, Series, and Products*, Academic Press, San Diego, 2000.
- [23] M. Keçeli, F.Ö. Ilday, and M.Ö. Oktel, *Phys. Rev. A* **75**, 035601 (2007).
- [24] E. Hairer and G. Wanner, *Solving Ordinary Differential Equations II: Stiff and Differential-Algebraic Problems*, Springer-Verlag, Berlin, 1996.
- [25] E. Giusti, *Direct Methods in the Calculus of Variations*, World Scientific, Singapore, 2003.
- [26] S. Inouye, M. R. Andrews, J. Stenger, H.-J. Miesner, D. M. Stamper-Kurn, and W. Ketterle, *Nature* **392**, 151 (1998).
- [27] F. K. Fatemi, K. M. Jones, and P. D. Lett, *Phys. Rev. Lett.* **85**, 4462 (2000).
- [28] Resonant energy transfer in Bose-Einstein condensates. A. I. Nicolin, M. H. Mogens, J. W. Thomsen, and R. Carretero-González. Submitted to *Physica D*, September 2007.
- [29] A. I. Nicolin, M. H. Mogens, and R. Carretero-González. *Phys. Rev. E*, **75** (2007) 036208.